CNPq

CBPF - CENTRO BRASILEIRO DE PESQUISAS FÍSICAS

Notas de Física

CBPF-NF-008/92

ANALYSIS OF ^{209}Bi and ^{238}U PHOTOFISSION CROSS SECTION IN THE QUASI-DEUTERON REGION OF PHOTONUCLEAR ABSORPTION

by

O.A.P. TAVARES and M.L. TERRANOVA

An analysis of the photofission reactions in the quasi-deuteron energy range of photonuclear absorption (~30-140 MeV) has been performed for ^{209}Bi and ^{238}U nuclei. Experimental cross section data available in the literature have been compared with calculated values obtained from a model in which the incoming photon is assumed to be absorbed by a neutron-proton pair (Levinger's quasi-deuteron photoabsorption), followed by a mechanism of evaporation-fission competition for the excited residual nuclei. The model has been shown to reproduce the main experimental features of ^{209}Bi and ^{238}U photofission cross section, although unexplained differences still remain in the case of ^{238}U-fission by 30-50 MeV incident photons.

PACS: 25.85. -w; 25.85.Jg

Key-words: Fission reactions; Photofission.

1. Introduction

The use of monochromatic photon beams of energy greater than 20 MeV or so to study photonuclear reactions has produced in the last twelve years a number of reliable data on photoreactions, particularly those concerned with fission reactions (photofission) of actinide nuclei [1-9] and, to a lesser extent, of heavy-metal nuclei of mass number A < 210 [8,10-14]. For incident photon energies in the range ∿30-140 MeV, the photofission data have been generally interpreted on the basis of a model which considers the primary nuclear photoabsorption as taking place between the incoming photon and a neutron-proton pair (quasi-deuteron photoabsorption mechanism first proposed by Levinger [15]) followed by a process of competition between nucleon evaporation and fission experienced by the excited residual nucleus [5,8,9,12-14,16,17]. This model, although strongly dependent on the values of some nuclear parameters (level density parameter, for instance) involved in the calculations, has shown to be capable in explaining the trend of fissility (total fission probability, f) with photon energy, k. In addition, at fixed moderate incident energies (k ≈ 50-70 MeV), the model has accounted for the existence of shell effects in fission which are clearly observed in the region of Z=82, N=126 shell closures when nuclear fissility is studied as a function of parameter Z^2/A of the target nucleus. Such effects have been put in evidence very recently [8,9].

Since a considerable number of measured photofission cross section data has been accumulated from bremsstrahlung-[18-23],

electron- [24-27], and monochromatic photon-induced [3-13] fission experiments, we thought it worthwhile to perform a detailed analysis of these data by evaluating the fission cross section, σ_f, as a function of energy from the referred current photofission model, and to compare it with the experimental results. Two representative target nuclei have been thus selected for the purposes of the present analysis, namely ^{209}Bi and ^{238}U. The reason for such a choice is twofold: first, among the nuclei which have been used to investigate photofission reactions, ^{209}Bi and ^{238}U are those for which the number of cross section data available in the range 30-140 MeV is the greatest; second, from a physical point of view, ^{209}Bi and ^{238}U exhibit a quite complete different fission response to incident photons in view of the extremely different values of fission barrier height of these two nuclei. In fact, ^{238}U shows a pronounced resonant-like structure in the fission cross section curve at photon energies $\lesssim$ 20 MeV, followed by an almost constant fission cross section at energies up to about 140 MeV; on the contrary, in the case of ^{209}Bi, the photofission cross section increases by several orders of magnitude from threshold ($k \approx 23$ MeV) on. The scope of the present analysis is to give a detailed description of the fission behavior for these two representative nuclei in the quasi-deuteron energy-range ($\sim$ 30-140 MeV) of photonuclear absorption.

2. Photofission cross section

In order to compare the calculated photofission cross section values with the measured ones, we constructed the curves

σ_f vs. k for ^{209}Bi and ^{238}U by taking the product of the total nuclear photoabsorption cross section, $\sigma_a^T(k)$, times the total fission probability (fissility, f(k)), i.e.,

$$\sigma_f(k) = \sigma_a^T(k) \times f(k) \quad . \tag{1}$$

The first quantity is evaluated from Levinger's modified quasi-deuteron model [28], according to which

$$\sigma_a^T(k) = L \frac{NZ}{A} \sigma_d(k) \exp(-D/k) \quad , \tag{2}$$

where $\sigma_d(k)$ is the total photodisintegration cross section of the free deuteron, NZ is the number of neutron-proton pairs in the nucleus, and L and D are, respectively, the so-called "Levinger's" and "damping" parameters, both depending on mass number A. A systematic study by Terranova et al. [29] of total nuclear photoabsorption cross section data taken in the range 35-140 MeV has shown that parameter D can be evaluated by $D=0.72A^{0.81}$ MeV, while from a very recent re-evaluation of Levinger's constant of nuclei throughout the Periodic Table by Tavares and Terranova [30] values of L have been calculated by $L=6.8-11.2A^{-2/3} + 5.7A^{-4/3}$. Finally, as far as $\sigma_d(k)$ is concerned, values have been taken from the recent fit to data compiled by Rossi et al. [31].

The second quantity in (1), f(k), is the quantity which gives all relevant physical differences in fission behavior for the nuclei under analysis. The development of a model and calculation method as well to obtain the values of f at each incident photon energy in the interval 30-140 MeV will be described in the next Section.

3. Calculation of nuclear fissility

Following the generally accepted, current two-step model for intermediate-energy photofission reactions, the incoming photon is firstly absorbed by a neutron-proton pair, the incident energy being shared between these two nucleons. Depending on their final kinetic energies inside the nucleus soon after the primary interaction, one of these nucleons, or both, may, or may not, escape from the struck nucleus leading to a residual nucleus with a certain excitation energy E^*, with a probability p. In a second stage, after termodynamic equilibrium was reached, fission will take place with a probability $P_f(E^*)$, as a result of a mechanism of competition between particle evaporation and fission experienced by the excited residual nucleus. Fissility is, therefore, obtained by multiplying these two referred probability values and summing up all possible modes of obtaining residual nuclei and of division of the incident energy by the neutron-proton pair. Since for each target nucleus and a fixed incident photon energy the quantities E^*, p, and $P_f(E^*)$ will depend on a quantity ζ suitable to describe the kinematics of the primary interaction through a function $g(k,\zeta)$, we can therefore write formally that

$$f(k) = \int_{\zeta_1}^{\zeta_2} \left[\sum_i p_i(k,\zeta) P_{f_i}(k,\zeta) \right] g(k,\zeta)\, d\zeta \Big/ \int_{\zeta_1}^{\zeta_2} g(k,\zeta)\, d\zeta \,, \qquad (3)$$

where $\sum_i p_i(k,\zeta) = 1$ always. Basically, the functions $g(k,\zeta)$, $p_i(k,\zeta)$, and $P_{f_i}(k,\zeta)$ describe, respectively, the primary interaction, the formation of the residual nucleus, and the

de-excitation of this latter leading to fission. These will be briefly discussed below.

The primary interaction is considered to occur between the incoming photon and a quasi-deuteron, where relativistic kinematics and the Pauli exclusion principle are applied to determine the kinetic energies of neutron and proton (respectively, T_{n*} and T_{p*}) in their final states. The angular distribution of the photointeraction with a quasi-deuteron (referred to the proton polar-angle in the center-of-mass system, θ') was considered, to a first approximation, to be the same as that for a free deuteron [32,33]. Preliminary calculations, however, have indicated that the assumption of isotropy ($d\sigma/d\Omega' = const.$) did not give significant differences in the final results of fissility as compared with calculations performed by taking the actual case of an anisotropic distribution ($\lesssim 3\%$ for ^{238}U and $\lesssim 5\%$ for ^{209}Bi). This result led us to consider "a priori" an isotropic angular distribution for the interaction $\gamma+(n+p)\rightarrow n^*+p^*$ throughout the calculations. In this way, the quantity ζ in (3) is identified as θ', and the function $g(k,\zeta)$ as $\sin\theta'$, from which (3) becomes

$$f(k) = \int_{\theta'_m}^{\theta'_M} \left[\sum_i p_i(k,\theta') P_{f_i}(k,\theta') \right] \sin\theta' d\theta' \Big/ (\cos\theta'_m - \cos\theta'_M) \quad , \qquad (4)$$

where the limiting angles θ'_m and θ'_M are determined from the restrictions imposed by the Pauli exclusion principle on the values of T_{n*} and T_{p*}.

Once the final neutron and proton kinetic energies referred to the nucleus system were determined as a result of

the primary interaction, a residual nucleus is considered to be formed following one of the three possible modes: i) the neutron escapes, at the same time that the proton remains within the nucleus; ii) the proton escapes with retention of the neutron; iii) both neutron and proton remain within the nucleus. There is, of course, a fourth possibility, namely, both neutron and proton escape simultaneously from the nucleus, but in this case no excitation energy is left to the residual nucleus, with the consequence of null fission probability. The condition for neutron escaping is $T_{n*} > E_c^n$, and for proton escaping $T_{p*} > E_c^p$, where E_c^n and E_c^p are the respective neutron and proton cut-off energies (see Table 1). The probabilities of escaping of nucleons (without suffering for any secondary interaction) are given by the nuclear transparencies to neutron and proton, which we shall denote, respectively, by τ_n and τ_p. Nucleon absorption, on the contrary, will occur if $T_{n*} \leq E_c^n$ or $T_{p*} \leq E_c^p$, and in both cases $\tau_n = \tau_p = 0$. The probabilities of absorption (i.e., non escaping) of neutron and proton are, respectively, $1-\tau_n$ and $1-\tau_p$. Therefore, the probability of formation of an excited residual nucleus following each of the three routes mentioned above is given by $p_1 = \tau_n(1-\tau_p)$, $p_2 = \tau_p(1-\tau_n)$, and $p_3 = (1-\tau_n)(1-\tau_p)$. Nuclear transparencies, which depend essentially on neutron and proton kinetic energies inside the nucleus, are thus the chief quantities to be used in evaluating in what proportion residual nuclei have been formed. The correspondent excitation energies are calculated as $E_1^* = k-T_{n*}+B_n$, $E_2^* = k-T_{p*}+B_p$, and $E_3^* = k$, where B_n and B_p are the binding energies, respectively, for neutron and proton.

In the final stage of the reaction, the de-excitation of the residual nucleus proceeds following a mechanism of competition between fission and particle evaporation. The significant de-excitation channels are neutron emission and fission, although a small contribution from proton and alpha-particle emission channels has been also considered at energies $E^* \gtrsim 80MeV$ for ^{209}Bi target nucleus (in the case of ^{238}U this contribution turns out inessential). In the present calculation not all sucessive chance fission probabilities have been included, but only the first-chance and the significant contribution due to the second-chance fission probability, in such a way that, starting from a certain residual nucleus (Z_i^*, A_i^*, E_i^*), $i = 1,2,3$ as before, the total fission probability expected for such a nucleus is obtained by

$$P_{f_i} = P^1_{f_i} + (1-P^1_{f_i})P^2_{f_i} \qquad (5)$$

(superscripts denote here the order of the chance fission.) Since for excitation energies up to 140 MeV neutron emission predominates strongly over proton and alpha-particle emissions, it was sufficient to consider for the second-chance fission a residual nucleus formed from its precedent by loosing of one neutron. Besides, from the kinetic energy distribution of evaporated neutrons, the excitation energy of the new residual has been considered, on the average, 10 MeV less than that of the precedent one.

So far, the above description has dealt, in a summary form, with the essentials and the basis of the method adopted to calculate nuclear fissility. Details will be seen in the

sub-sections below.

3.1. *Nuclear model and kinematics of the primary interaction*

The nucleus is considered to be a degenerate Fermi gas of non-interacting neutrons and protons confined within a spherically symmetric nuclear potential of radius R, the value of which is given by the equivalent root-mean-square radius of the nuclear charge distribution (see Table 1). The Fermi energies for neutrons (E_F^n) and protons (E_F^p), as well as the respective cut-off energies (E_c^n and E_c^p), have been calculated by the usual way, and the values used for these quantities are listed in Table 1.

To calculate the kinetic energies of neutron (T_{n*}) and proton (T_{p*}) after nuclear photoabsorption by a neutron-proton pair, the following simplifying assumptions are made: i) neutrons and protons move at random in their respective Fermi gases; ii) the kinetic energy distributions of neutrons and protons before the interaction are replaced by the respective average Fermi energies, in such a way that the kinetic energies of the neutron and proton in the initial state are considered constant and equal to

$$T_n = T_p = T = (1/2)\left[(3/5)E_F^n+(3/5)E_F^p\right] = (3/10)(E_F^n+E_F^p) \quad . \qquad (6)$$

The relativistic energy-momentum conservation laws applied to the interaction $\gamma+(n+p) \rightarrow n^*+p^*$ give, for the total energy available in the center-of-mass (CM) system,

$$E' = \left\{2\left[m^2+(T+m)(2k+T+m)-\vec{k}.(\vec{p}_n+\vec{p}_p)-\vec{p}_n.\vec{p}_p\right]\right\}^{1/2} \quad , \qquad (7)$$

where $\vec{k}$, $\vec{p}_n$ and $\vec{p}_p$ are the initial momenta, respectively, of the photon, neutron, and proton as referred to the nucleus system, and m is the nucleon rest mass expressed in energy units. The transformation back from the CM to the nucleus system yields the following result for neutron and proton kinetic energies in the final state

$$T_{n*} = a(1-b\cos\theta') - m \qquad (8)$$

$$T_{p*} = a(1+b\cos\theta') - m \qquad (9)$$

in which

$$a = T + m + k/2 \qquad (10)$$

$$b = \{[1-(2m/E')^2][1-(E'/(k+2T+2m))^2]\}^{1/2} \quad . \qquad (11)$$

In these expressions θ' is the polar-angle of the proton direction in the final state as referred to the CM-system, and, in view of the assumption i) above, E'^2 is replaced by the average value of the square of the quantity expressed by (7), the value of which is calculated as

$$\overline{E'^2} = 2\,[m^2+(T+m)(2k+T+m)] \quad . \qquad (12)$$

Note that whatever θ', $T_{n*}+T_{p*} = k+(3/5)(E_F^n+E_F^p)$. Since the primary interaction can only take place if $T_{n*} > E_F^n$ and $T_{p*} > E_F^p$, it follows that the present model is applicable only to photon energies $k \gtrsim 26$ MeV in the case of ^{209}Bi and ^{238}U target nuclei. Figure 1 shows two illustrative examples of how is the photon energy shared between neutron and proton after the primary interaction with a quasi-deuteron.

As a practical consequence for the routine of calcul-

ations, it was useful to transform in (4) variable θ' into T_{n*}. From (8) we have $\sin\theta' d\theta' = dT_{n*}/(ab)$, and $\cos\theta'_m - \cos\theta'_M = (T^M_{n*} - T^m_{n*})/(ab)$. Since the new limits are $T^m_{n*} = E^n_F$ and $T^M_{n*} = k + (3E^n_F - 2E^p_F)/5$, it follows that $\cos\theta'_m - \cos\theta'_M = [k - 2(E^n_F + E^p_F)/5]/(ab)$. By substituting these results into (4) we therefore obtain

$$f(k) = \int_{E^n_F}^{k+(3E^n_F-2E^p_F)/5} \left[\sum_{i=1}^{3} p_i(k,T_{n*}) P_{f_i}(k,T_{n*})\right] dT_{n*}/[k-2(E^n_F+E^p_F)/5] \quad . \tag{13}$$

This is the final formula from which fissility values have been calculated as a function of photon energy. Thus, the basic assumptions of motion of neutrons and protons at random before the primary interaction, and isotropy in the CM angular distribution make the evaluation of the details of the kinematics of the primary interaction unnecessary, in such a way that all the subsequent quantities to be used in calculating fissility can be expressed as functions of T_{n*}, which is allowed to vary continuously in the interval $E^n_F \leq T_{n*} \leq k + (3E^n_F - 2E^p_F)/5$.

3.2. *Nuclear transparencies and excitation energy of the residual nucleus*

Nuclear transparency is the chief quantity to evaluate the probabilities of excitation of the residual nuclei. It gives the probability of a nucleon to escape from the nucleus without suffering for any secondary interactions. This problem was solved in the past by several authors [36-40] who used different approaches to obtain closed formulae or Monte Carlo calculation for evaluation of nuclear transparencies to both nucleons and pions produced within the nucleus. In the present analysis option has

been made for the formalism developed by de Carvalho et al. [38] based on the optical model and on the idea of an equivalent nucleus, i.e., a nucleus for which the transparency to a particle coming from outside is the same as the transparency to the same particle but emerging from inside the nucleus. Accordingly,

$$\tau_j = \left[\lambda_j^2/(2R'^2)\right] \times \left[1-(1+2R'/\lambda_j)\exp(-2R'/\lambda_j)\right] \quad , \quad j=n \text{ or } p, \qquad (14)$$

where $R' = 0.589R$ is the radius of the equivalent nucleus (R is that of the actual nucleus), and $\lambda_j = (\rho\bar{\sigma}_j)^{-1}$ is the mean-free-path of particle j in nuclear matter. Here, ρ is the nucleon density, and $\bar{\sigma}_j$ is the average total cross section for interaction of particle j with a nucleon. This latter is calculated as

$$\bar{\sigma}_j = \left[Z\sigma_{jp}^b + (A-Z)\sigma_{jn}^b\right]/A \quad , \qquad (15)$$

where σ_{jp}^b and σ_{jn}^b are the total cross sections for the interaction of particle j with, respectively, a bound proton and a bound neutron, i.e., cross sections corrected for nucleon motion and the Pauli exclusion principle. Such "bound" nucleon-nucleon cross sections have been obtained from the respective "free" nucleon-nucleon cross sections by the method developed by Kikuchi and Kawai [41]. The result is

$$\sigma^b = \sigma^f \times P_B(y) \quad , \quad y = E_F/T \quad , \qquad (16)$$

where, for kinetic energies $T \lesssim 150$ MeV, the correction factor $P_B(y)$ can be calculated to good approximation by the relationship (the so-called "approximation B" of Kikuchi and Kawai [41])

$$P_B(y) = \begin{cases} 1 - 1.44y \quad , & 0 \leq y \leq 1/2 \\ 1 - 1.44y + 0.44y(2-1/y)^{2.17} \quad , & 1/2 < y \leq 1 \ . \end{cases} \tag{17}$$

By making further the approximation $\sigma^f_{nn} = \sigma^f_{pp}$, and using the fact that $\sigma^f_{pn} = \sigma^f_{np}$, the precedent equations can be handled to give the following result for the nuclear transparencies to emergent neutrons and protons:

$$\tau_j = (2530/x_j^2)\left[1-(1+u_j)\exp(-u_j)\right] \ , \quad u_j = 0.0281277x_j \ , \quad j=n \text{ or } p \ , \tag{18}$$

where

$$x_n = \frac{Z\sigma^f_{np} + (A-Z)\sigma^f_{pp}}{R^2} \times P_B(E^n_F/T_{n*}) \tag{19}$$

$$x_p = \frac{(A-Z)\sigma^f_{np} + Z\sigma^f_{pp}}{R^2} \times P_B(E^p_F/T_{p*}) \tag{20}$$

in which cross sections are expressed in mb, and nuclear radius in fm. The values of the "free" nucleon-nucleon cross sections used throughout the calculations have been taken from the smoothed curves reported by Metropolis et al. [42]. Figure 2 shows the values of transparency for ^{209}Bi and ^{238}U nuclei to emergent neutrons and protons as obtained by the method described above.

The distributions of excitation energy can be now constructed for the different possible modes of formation of residual nuclei following the procedure outlined in Section 3. An example of such distributions is given in Fig. 3, where the case for absorption of a 85-MeV incident photon by a ^{209}Bi target is considered. In this example it is seen that simultaneous escaping of neutron and proton occurs in 3.3% of cases (Fig.3-a);

neutron alone has a 29% chance of escaping,producing a residual nucleus with ∿ 26 MeV of average excitation energy (Fig. 3-b); for escaping of the proton, these figures become 6% and ∿ 23 MeV (Fig. 3-c); finally, neutron and proton remain simultaneously absorbed within a ^{209}Bi target in almost 62% of cases, in which the excitation energy equals to the photon incidente energy of 85 MeV (Fig. 3-d).

3.3. *Partial fission probabilities*

The residual nuclei which are formed after escaping or absorption of the neutron and/or proton participating in the primary interaction de-excite by a mechanism of competition between particle evaporation and fission. As stated before,along with neutron emission, proton and alpha-particle emissions may also compete to some extent with the fission mode, specially in those cases where fission barrier is comparable with Coulomb--plus-separation energy of the particle. Thus, working in a systematic way, the partial fission probabilities have been calculated by

$$P_f = F/(1+F+G+H) \quad , \tag{21}$$

where F, G, and H represent, respectively, the probability of fission, proton emission, and alpha-particle emission relative to neutron emission. Expressions for these three quantities have been obtained from the statistical model by Weisskopf [43] and Vendenbosch and Huizenga [44]:

$$F= \frac{15[2r^{1/2}.a_n^{1/2}.(E^*-B_f)^{1/2}-1]}{4r\,A^{2/3}(E^*-B_n)} \exp\left\{2a_n^{1/2}\left[r^{1/2}(E^*-B_f)^{1/2}-(E^*-B_n)^{1/2}\right]\right\}; \tag{22}$$

$$G = \frac{E^*-B_p-V_p}{E^*-B_n} \exp\left\{2a_n^{1/2}\left[(E^*-B_p-V_p)^{1/2}-(E^*-B_n)^{1/2}\right]\right\} \quad ; \qquad (23)$$

$$H = \frac{2(E^*-B_\alpha-V_\alpha)}{E^*-B_n} \exp\left\{2a_n^{1/2}\left[(E^*-B_\alpha-V_\alpha)^{1/2}-(E^*-B_n)^{1/2}\right]\right\} \quad ; \qquad (24)$$

in which

$$B_f = CB_{f_0} \quad ; \quad V_p = CV_{p_0} \quad ; \quad V_\alpha = CV_{\alpha_0} \quad , \qquad (25)$$

where $C = 1-E^*/B$ is a correction factor which takes into account for nuclear temperature effects [45]. Most of the quantities appearing in the above equations, and the values used in the calculations for the various residual nuclei as well, are defined in Table 2. The Coulomb barriers for proton and alpha particle at the nuclear surface have been calculated, respectively, by

$$V_{p_0} = \frac{\kappa_p(Z-1)e^2}{r_0(A-1)^{1/3}+1.14} \quad \text{MeV} \qquad (26)$$

$$V_{\alpha_0} = \frac{2\kappa_\alpha(Z-2)e^2}{r_0(A-4)^{1/3}+2.16} \quad \text{MeV} \quad , \qquad (27)$$

where $\kappa_p = 0.70$ and $\kappa_\alpha = 0.83$ are the penetrabilities through the barriers, the values of which having been chosen following the work by LeCouteur [47]; $r_0 = 1.20$ fm is the nuclear radius parameter as deduced from the systematics of charge radii by Myers and Schimidt [48]; $e^2 = 1.44$ MeV.fm is the square of the electron charge, and 1.14 fm and 2.16 fm are the equivalent root-mean-square radii of the charge distribution, respectively, for proton and alpha particle as evaluated from data compiled by Brown et al.[34].

For the level-density parameter of the residual nucleus after neutron evaporation, a_n, it has been adopted the expression proposed by Iljinov et al. [16], which incorporates corrections

due to excitation energy and shell effects as well. Accordingly,

$$a_n=(0.134A-1.21\times10^{-4}A^2)\left\{1+[1-\exp(-0.061E^*)]\Delta M/E^*\right\}\ \text{MeV}^{-1}, \qquad (28)$$

where ΔM is the shell correction to the nuclear mass (Table 2).

The quantity $r = a_f/a_n$ represents the ratio of the level-density parameter at the fission saddle point to a_n. Since the final results of calculated fissility are very sensitive to the values of r, it is essential to obtain an evaluation of the r-values as accurate as possible. Calculations have indicated that, although not negligible, the contributions $p_1P_{f_1}$ and $p_2P_{f_2}$ to the sum $\sum_{i=1}^{3} p_iP_{f_i}$ in (13) have shown small. Thus, we can write to a first approximation that

$$f(k) \approx P^1_{f_3}(k)\times\bar{p}_3(k) \qquad , \qquad (29)$$

i.e., fissility is given approximately by the first-chance fission probability of the target nucleus excited to E^*_3 = k times the average probability for this mode of excitation to occur (like the example showed in Fig. 3-d). $p_3 = (1-\tau_n)(1-\tau_p)$, so that $\bar{p}_3$ is easily obtained from nuclear transparencies to neutron and proton in the energy interval allowed for T_{n^*} at each fixed value of k. Finally, semi-empirical values of $r = a_f/a_n$ can be obtained by solving (29) in such a way that experimental fissilities ($\sigma_f^{exper.}/\sigma_a^T$) be reproduced. The above procedure has been applied to photofission data of ^{209}Bi in the range 30-140 MeV, and, surprisingly, results have indicated that the ratio a_f/a_n decreases with increasing of excitation energy in such a proportion that a_f remains rather independent of excitation energy. Assuming this result is also valid for the other residual nuclei which are

formed successively after the primary photoabsorption by ^{209}Bi and ^{238}U targets, it was possible to deduce a closed formula to evaluate a_f within 1-2% accuracy, and hence $r = a_f/a_n$ to be inserted into (22). By making use of the appropriate expressions for $r = a_f/a_n$ previously obtained at 69-MeV excitation energy [8], it follows that

$$a_f=[1+0.05917(Z^2/A-34.34)](1+0.0143\Delta M)(0.134A-1.21\times10^{-4}A^2)\ MeV^{-1},$$
$$Z^2/A \gtrsim 34.90 \qquad (30)$$

$$a_f=[1+0.08334(Z^2/A-30.30)](1+0.0143\Delta M)(0.134A-1.21\times10^{-4}A^2)\ MeV^{-1},$$
$$31.20 < Z^2/A \lesssim 34.00 \quad , \qquad (31)$$

where ΔM is expressed in MeV. The dependence of $r = a_f/a_n$ on excitation energy obtained in this way is depicted in Fig. 4 for some selected residual nuclei, which shows results consistent with data reported in the literature [44].

The trends of fission probability with excitation energy for the first three residual nuclei formed after the primary interaction are shown in Fig. 5 (^{209}Bi target) and Fig. 6 (^{238}U target). In the former case, the calculated fission probabilities increase very steeply at low excitation energies, exhibiting an asymptotic behavior as nuclear excitation increases from about 60 MeV; many orders of magnitude are displayed according to the different residual nuclei as excitation increases from threshold up to 140 MeV (Fig. 5). This is the typical behavior of fission probability of nuclei located in the Pb-Bi region, caused by a relatively large value (22-24 MeV) of the height of fission barrier of these nuclei. On the contrary, in the case of ^{238}U

target nucleus, since the fission barriers of the residual nuclei are not too high ($\sim$5 MeV), the trends are quite different (Fig.6), showing values of fission probability near unity, with minima in the curves P_f vs. E*, as consequence of the strong competition with neutron evaporation.

4. Results and comparison with experimental data

For the sake of clarity, we present first the variation of the three quantities of interest (σ_a^T, f, and σ_f) with photon energy as obtained in the present analysis. Figures 7 and 8 show these results, respectively, for ^{209}Bi and ^{238}U. The trends of σ_a^T are very similar to each other (solid curves in part a)); for ^{209}Bi a decrease in σ_a^T of about 36% is noted as one goes from 30 up to 140 MeV, whereas for ^{238}U it reduces to about 27%. Some experimental data are also shown to allow a comparison with the calculated trends. These data were taken from the measurements by Leprêtre et al. [49]. Since unfortunately such data are not available for Bi, we decided in this case to represent the Pb data of [49] in view of the strong dependence of σ_a^T with mass number (cf. (2)). For both Bi and U cases quite good agreement is indeed observed between calculated and experimental results.

Nuclear fissility is represented in part b) of Figs. 7 and 8. In the case of ^{209}Bi (Fig. 7) fissility increases monotonically from about 10^{-5} up to 10^{-1}, reflecting the trends of the partial fission probabilities discussed before (cf. Fig. 5). For ^{238}U (Fig. 8) fissility first decreases from a value near 1 down to $\sim$0.5, then it increases asymptotically towards 0.9,

showing that fission predominates over neutron emission at incident photon energies beyond 60 MeV. The apparent minimum around 40 MeV comes from the main contributions to fissility due to the residuals ^{237}U and ^{238}U, for which residuals fission probability has a minimum (cf. Fig. 6).

Finally, the product $\sigma_a^T \times f$ at each energy k gives the photofission cross section curves, $\sigma_f(k)$, depicted in part c) of Figs. 7 and 8, which curves we shall compare with the experimental data.

Figure 9 shows the case for $^{209}Bi(\gamma,F)$. The calculated trend obtained from the model discussed in the precedent Sections (solid curve) can be considered in substantial agreement with both the low- and high-energy cross section data, especially with the data taken from electron- and monochromatic photon-induced fission experiments. As one can see, the model is able at reproducing a variation of four orders of magnitude displayed by the measured photofission cross section. Some disagreement is noted, however, in the range $\sim$70-120 MeV, where the calculated cross section differs from the measured one by an average factor of 2. Such a discrepancy may be ascribed mainly to difficults in defining a more accurate dependence of the quantity a_f (and so a_f/a_n) on excitation energy (cf. (31)).

The case for ^{238}U is presented in Fig. 10. Most of the experimental cross section data is dispersed within the interval 10-20 mb, showing that the cross section is not well defined in the energy range 30-140 MeV. The measurements by Leprêtre et al. [5] (open circles) constitute the unique comprehensive set of data covering the region 40-105 MeV, these data being compatible with a constant mean value of 16±2 mb, in good agreement with

Monte Carlo calculations at energies up to 75 MeV (solid curve from [5]). For photon energies beyond ∿ 60 MeV, the result of the present calculation (dashed curve) agrees quite well with that reported in [5], although marked differences there exist at the lower energies. In particular, neither the experimental data nor the Monte Carlo calculation by Leprêtre et al. [5] are reproduced by the calculated curve of the present work in the range ∿ 30-50 MeV. It is, however, interesting to note a decrease in the cross section showed by the measurements by Arruda-Neto et al.[25] (dash-dotted curve). At the higher energies ($k \gtrsim 110$ MeV), but below the meson photoproduction threshold, the present calculated cross section equals to about 12 mb, thus differing from most of data by ∿ 40%. However, at these energies, the available measured photofission cross sections pass beyond the total nuclear photoabsorption cross sections by ∿ 10-56%. Although serious difficults there still exist in obtaining both experimental and calculated results, the data for ^{238}U as a whole show that the photofission cross section is rather independent on incident photon energy, and that it amounts to about 80-90% of the total reaction channel in the quasi-deuteron region of photonuclear absorption.

5. Summary and conclusion

In the course of the present work, photofission cross section data of ^{209}Bi and ^{238}U nuclei available at energies covering the quasi-deuteron region of photonuclear absorption (30-140 MeV) have been analysed and interpreted on the basis of a model which considers a primary photointeraction with neutron-

-proton pairs followed by a de-excitation process of the residual nucleus in which particle evaporation competes with fission. A Fermi gas of neutrons and protons has been assumed for the target nucleus, and the Pauli exclusion principle has been used throughout in evaluating the neutron and proton kinetic energies after the primary photointeraction. The distributions of excitation energy of the residual nuclei have been constructed from calculated nuclear transparencies to neutrons and protons based on the optical model and on the concept of an equivalent nucleus. Neutron, proton and alpha particle emissions have been considered, in a systematic way, to compete with fission during the stage of de-excitation of the residual nucleus. First- and second-chance fission probabilities have been taken into account throughout the calculations, and appropriate semi-empirical formulae for evaluating the level-density parameters have been introduced in order to obtain fissility values as accurate as possible. Calculated photofission cross sections have been then compared with experimental data, and satisfactory agreement has been found at various incident photon energies on both ^{209}Bi and ^{238}U targets, although discrepancies there still exist, particularly in the low-energy (30-50 MeV) photofission of ^{238}U.

In spite of the uncertainties associated with both the measured and calculated results, the model developed in the present work has accounted for the main features of the observed trend of photofission cross section. Future work on this line is of course needed for to clarify some physical aspects of the photofission behavior which have not been explained yet.

Figure Captions

Fig. 1. Illustrating the division of incident photon energy, k, into neutron and proton kinetic energies, T_{n*} and T_{p*}, after absorption of the incoming photon by a neutron-proton pair (quasi--deuteron) inside the target nucleus. The cases for a 50-MeV (a) and 140-MeV (b) incident photon on ^{238}U are shown. Neutron and proton Fermi energies, E_F^n and E_F^p, are indicated to show the range of proton CM-angle, θ', within which the primary interaction is allowed according to the Pauli exclusion principle.

Fig. 2. Calculated transparency of ^{209}Bi and ^{238}U nuclei to emergent neutron, τ_n, and proton, τ_p, as a function of kinetic energy inside the nucleus.

Fig. 3. Distribution of excitation energy of the residual nuclei which are formed after the primary photoabsorption by a quasi--deuteron. It is shown the case for a 85-MeV incident photon on ^{209}Bi target nucleus. The percentage of formation of the different residual nuclei are indicated for the example considered.

Fig. 4. The ratio $r = a_f/a_n$ is plotted against excitation energy of the residual nucleus. The numbers near the curves refer to different residual nuclei as indicated.

Fig. 5. Calculated first-chance fission probability plotted against excitation energy of the residual nuclei which are formed after absorption of the incoming photon in a ^{209}Bi target nucleus.

Fig. 6. The same as in Fig. 5 for ^{238}U target nucleus.

Fig. 7. Total nuclear photoabsorption cross section, σ_a^T (part a), nuclear fissility, f (part b), and photofission cross section, σ_f (part c), plotted against incident photon energy, k, for ^{209}Bi. The curve in part a) is the result obtained from Levinger's modified quasi-deuteron model (equation (2)), and the experimental points (referred to Pb) have been taken from [49]; the curve in part b) results from the present photofission model as discussed

in the text; in part c), $\sigma_f = f \times \sigma_a^T$.

Fig. 8. The same as in Fig. 7 for ^{238}U. Experimental data in part a) have been taken from [49].

Fig. 9. Comparison between calculated and experimental photofission cross section data for ^{209}Bi in the range 30-140 MeV. The calculated trend (full line, present work) is reproduced from Fig. 7-c. Experimental data are as follows: ○ , Lemke et al. [10]; ---, Türck et al. (quoted in [10]); ● , Martins et al. [8]; ▲ , Minarik and Novikov [20]; ·-·-·-, Arruda-Neto et al. [26]; □ , Moretto et al. [24]; ◎, Martins et al. [13]; △ , Jungerman and Steiner [19]; ◑ , Bernardini et al. [18]; ■ , Bellini et al. [11]; ◇ , Vartapetyan et al. [22]; ▽ , Guaraldo et al. [12]; ▼ , Warnock and Jensen [21].

Fig. 10. Comparison between calculated and experimental photofission cross section data for ^{238}U in the range 30-140 MeV. The dashed line is the calculated trend as obtained in the present work (cf. Fig. 8-c); the full line is the result of the Monte Carlo calculation by Leprêtre et al. [5]. Experimental data are as follows: ◪ , Bellini et al. [23]; ◑ , Bellini et al. [4]; ○ , Leprêtre et al. [5]; □ , Moretto et al. [24]; ◊ , Ivanov et al. [7]; ▽ , Ahrens et al. [3]; △ , Minarik and Novikov [20]; ● , Bernabei et al. [6]; ■ , Martins et al. [8]; ▲ , Tavares et al. [9];-·-·-·, Arruda-Neto et al. [25].

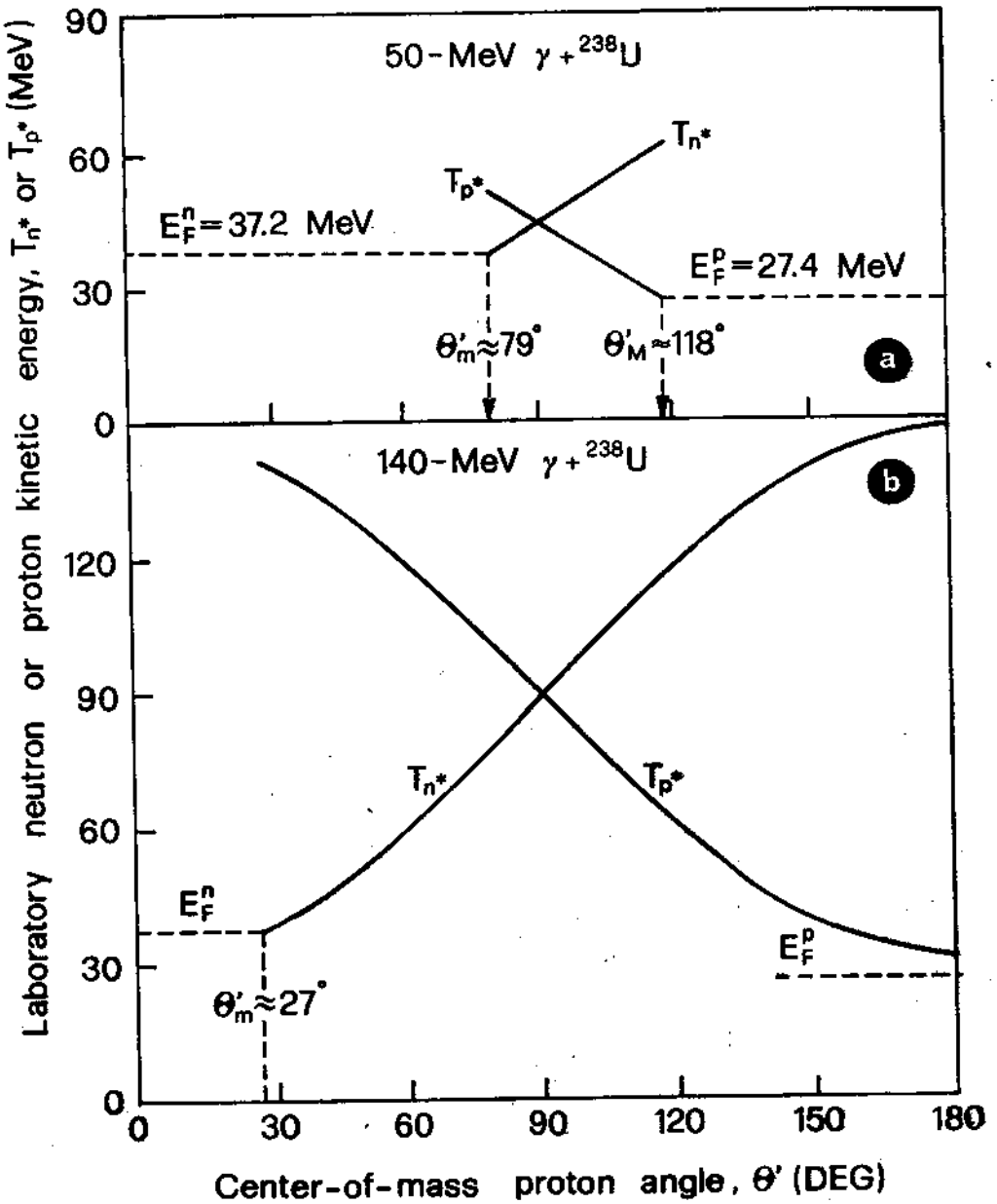
50-MeV γ + 238U
Tn*
Tp*
E_F^n = 37.2 MeV
E_F^p = 27.4 MeV
θ'm ≈ 79°
θ'M ≈ 118°
a
140-MeV γ + 238U
b
Tn*
Tp*
E_F^n
E_F^p
θ'm ≈ 27°
Laboratory neutron or proton kinetic energy, Tn* or Tp* (MeV)
Center-of-mass proton angle, θ' (DEG)
0
30
60
90
120
150
180

FIG. 1

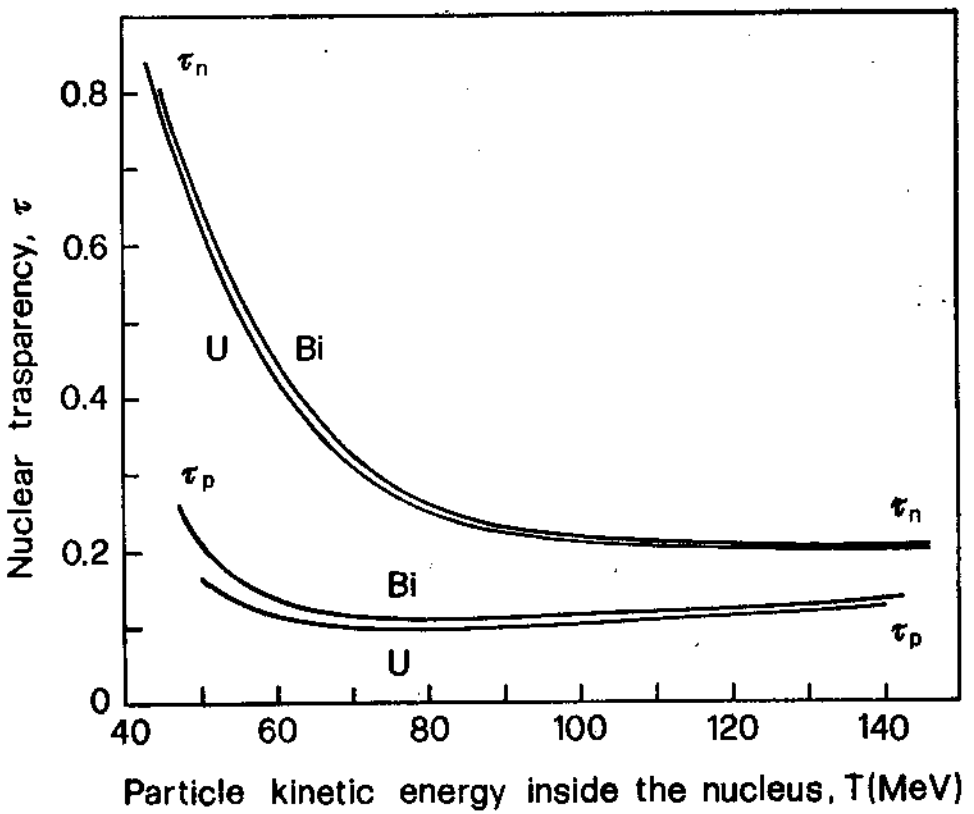
Nuclear trasparency, τ
0.8
0.6
0.4
0.2
0
40
60
80
100
120
140
Particle kinetic energy inside the nucleus, T(MeV)
τn
U
Bi
τp
Bi
U
τn
τp

FIG. 2

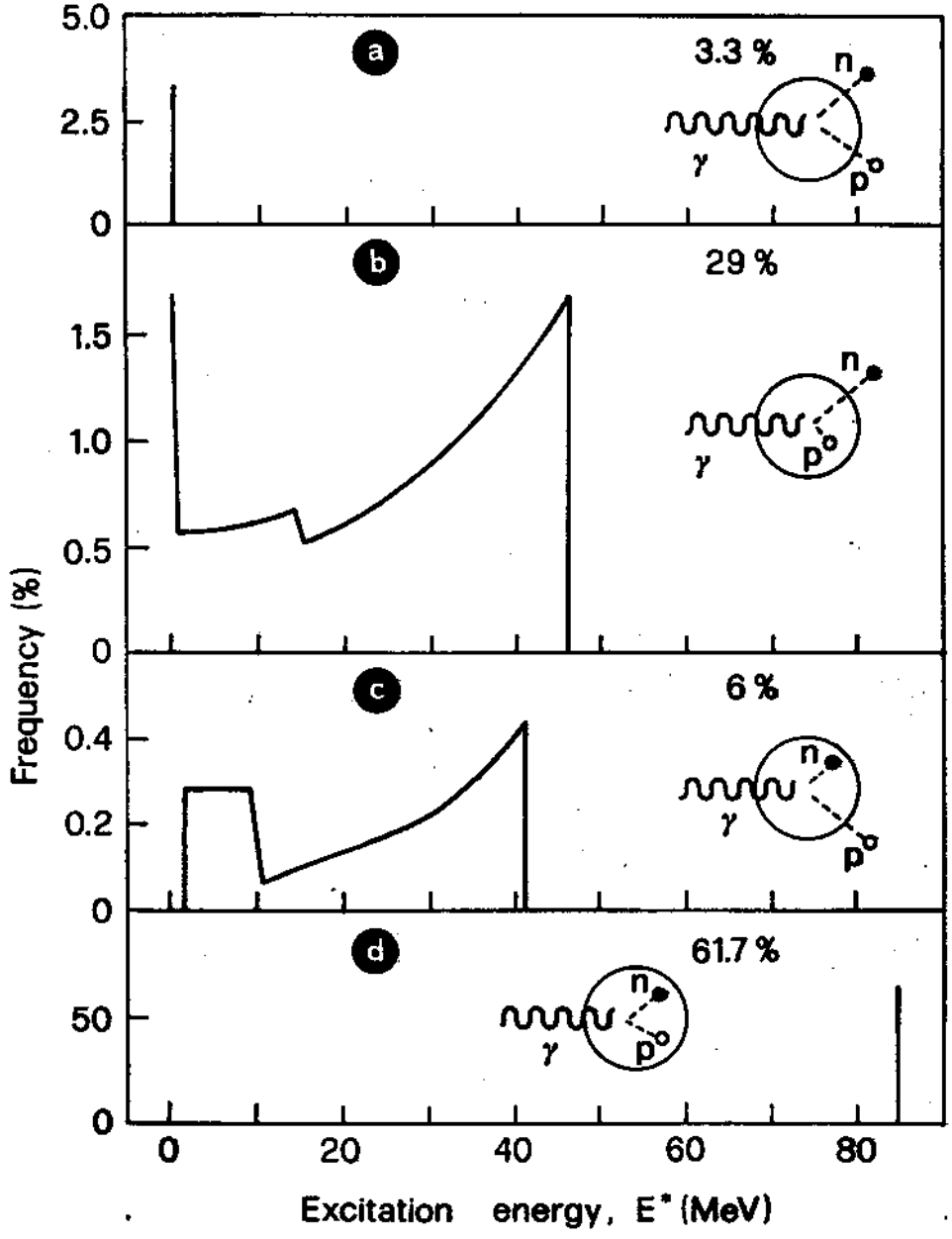
a
3.3 %
n
γ
p°
b
29 %
n
γ
p°
c
6 %
n
γ
p°
d
61.7 %
n
γ
p°
5.0
2.5
0
1.5
1.0
0.5
0
0.4
0.2
0
50
0
0
20
40
60
80
Frequency (%)
Excitation energy, E* (MeV)

FIG. 3

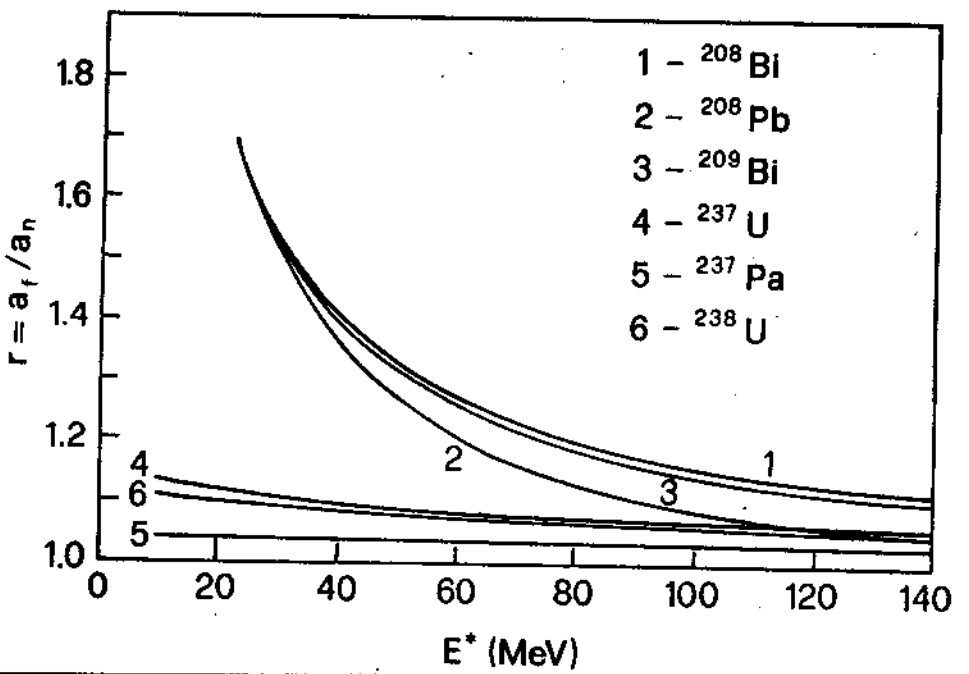
1 - 208 Bi
2 - 208 Pb
3 - 209 Bi
4 - 237 U
5 - 237 Pa
6 - 238 U
r = a_f / a_n
E* (MeV)
1.8
1.6
1.4
1.2
1.0
0
20
40
60
80
100
120
140

FIG. 4

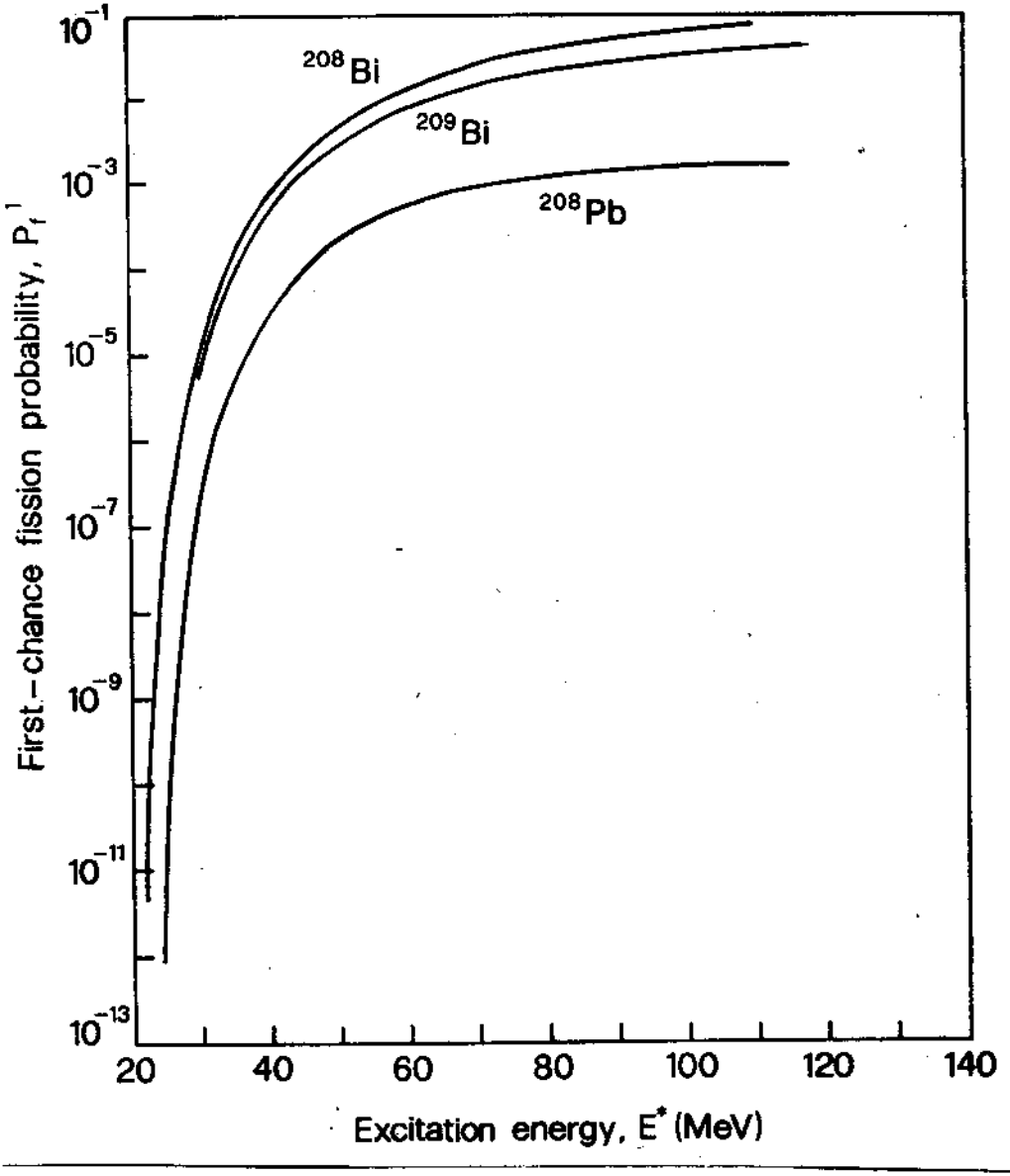
10^{-1}
10^{-3}
10^{-5}
10^{-7}
10^{-9}
10^{-11}
10^{-13}
First-chance fission probability, P_f^1
^{208}Bi
^{209}Bi
^{208}Pb
20
40
60
80
100
120
140
Excitation energy, E^* (MeV)

FIG. 5

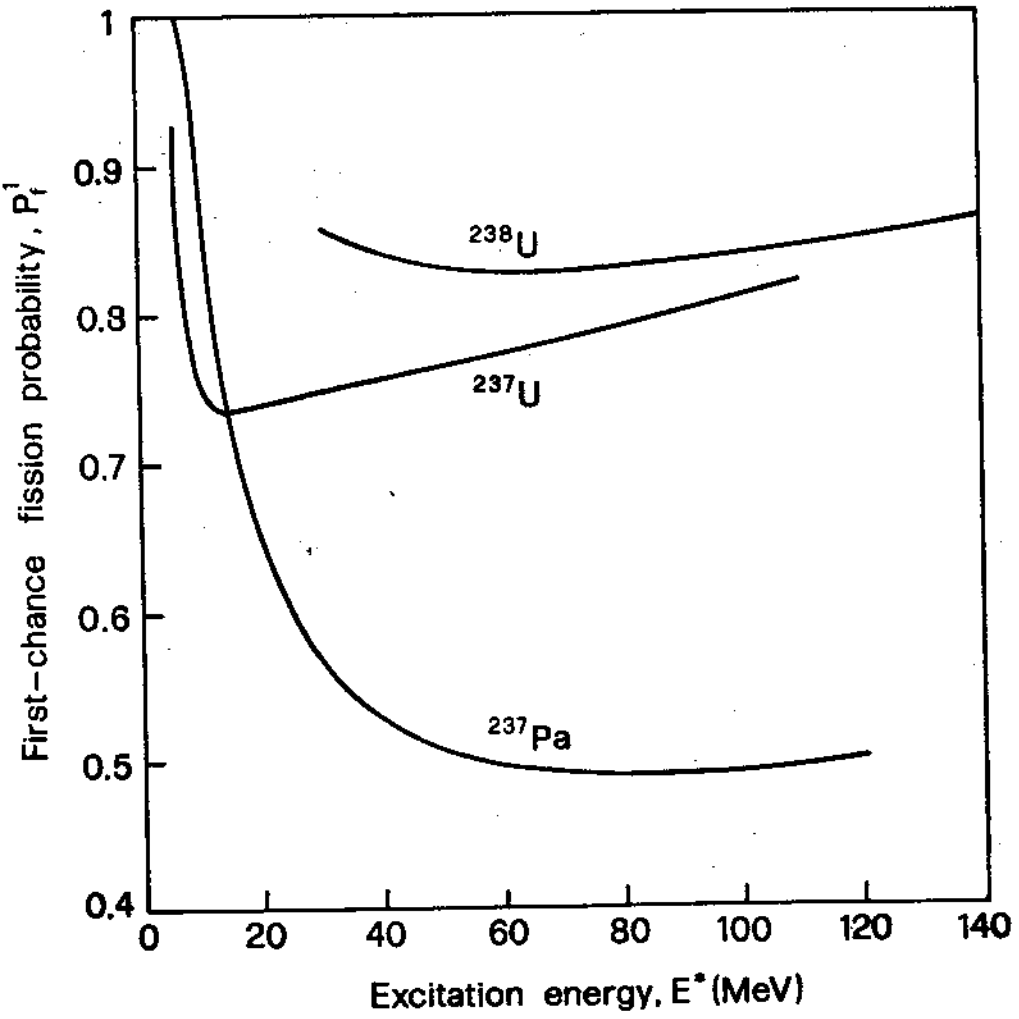
First-chance fission probability, P_f^1
1
0.9
0.8
0.7
0.6
0.5
0.4
0
20
40
60
80
100
120
140
Excitation energy, E^* (MeV)
^{238}U
^{237}U
^{237}Pa

FIG. 6

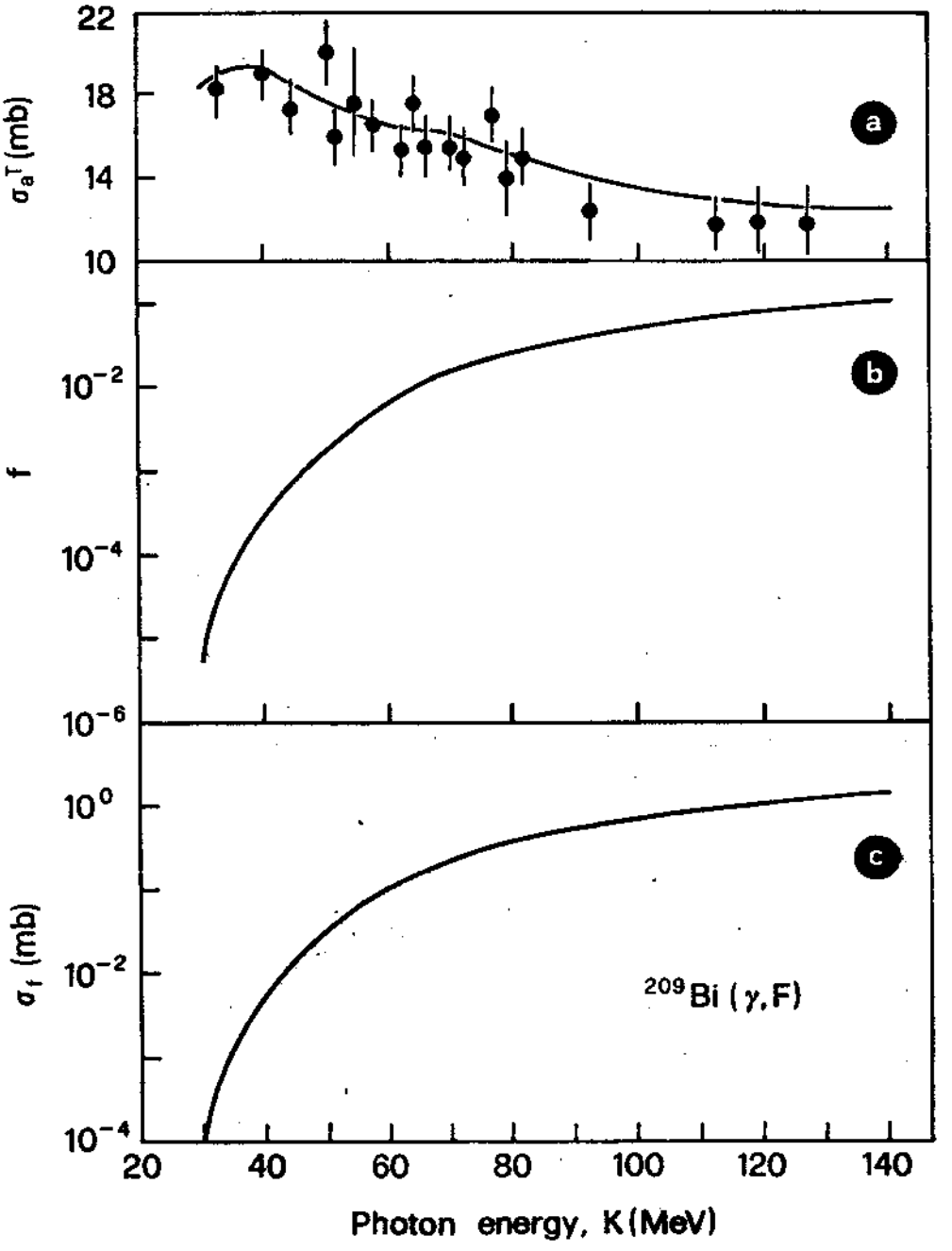
22
18
14
10
σ_a^T (mb)
a
10^{-2}
10^{-4}
10^{-6}
f
b
10^0
10^{-2}
10^{-4}
σ_f (mb)
c
^{209}Bi (γ,F)
20
40
60
80
100
120
140
Photon energy, K(MeV)

FIG. 7

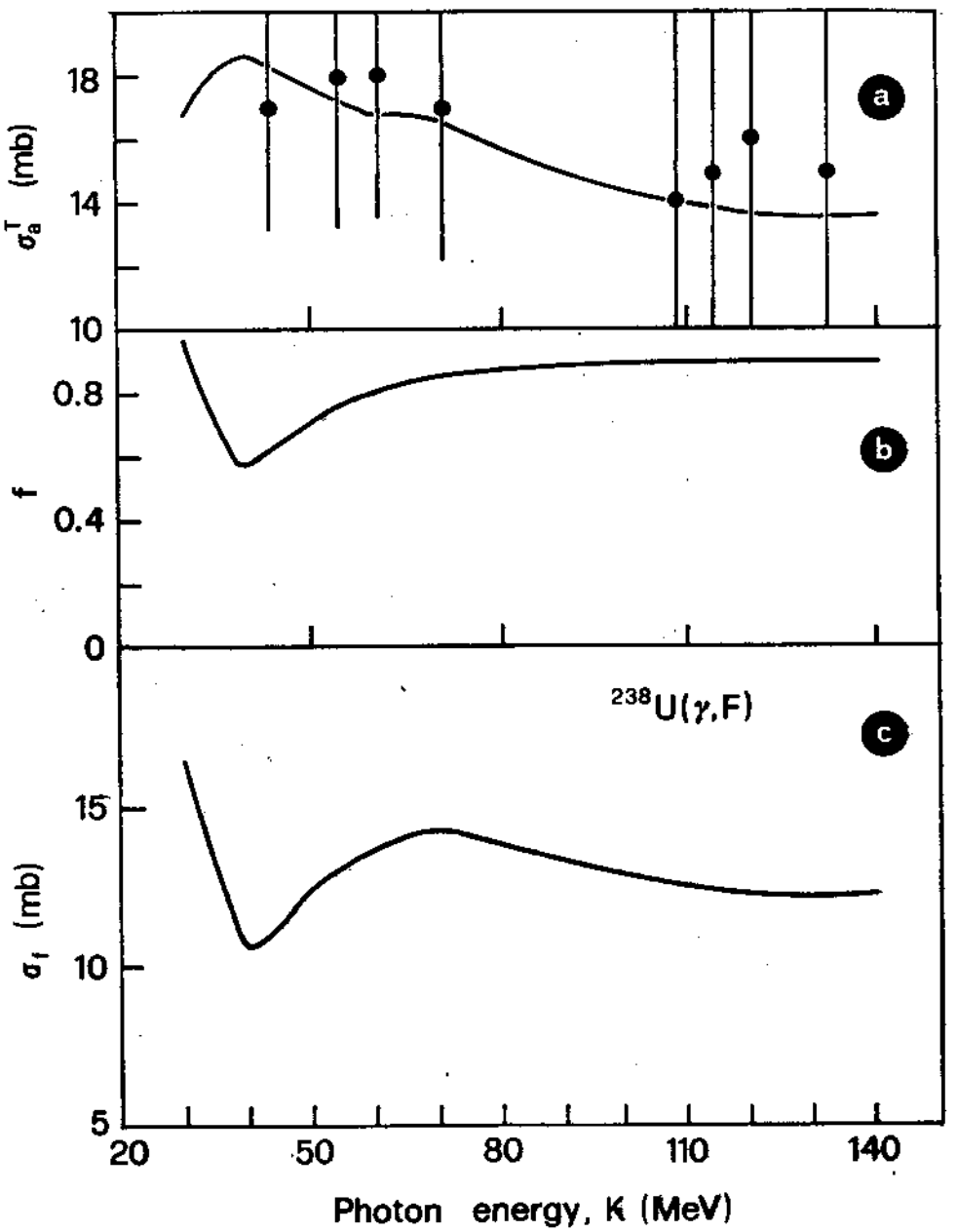
18
14
10
σ_a^T (mb)
a
0.8
0.4
0
f
b
$^{238}U(\gamma,F)$
c
15
10
5
σ_f (mb)
20
50
80
110
140
Photon energy, K (MeV)

FIG. 8

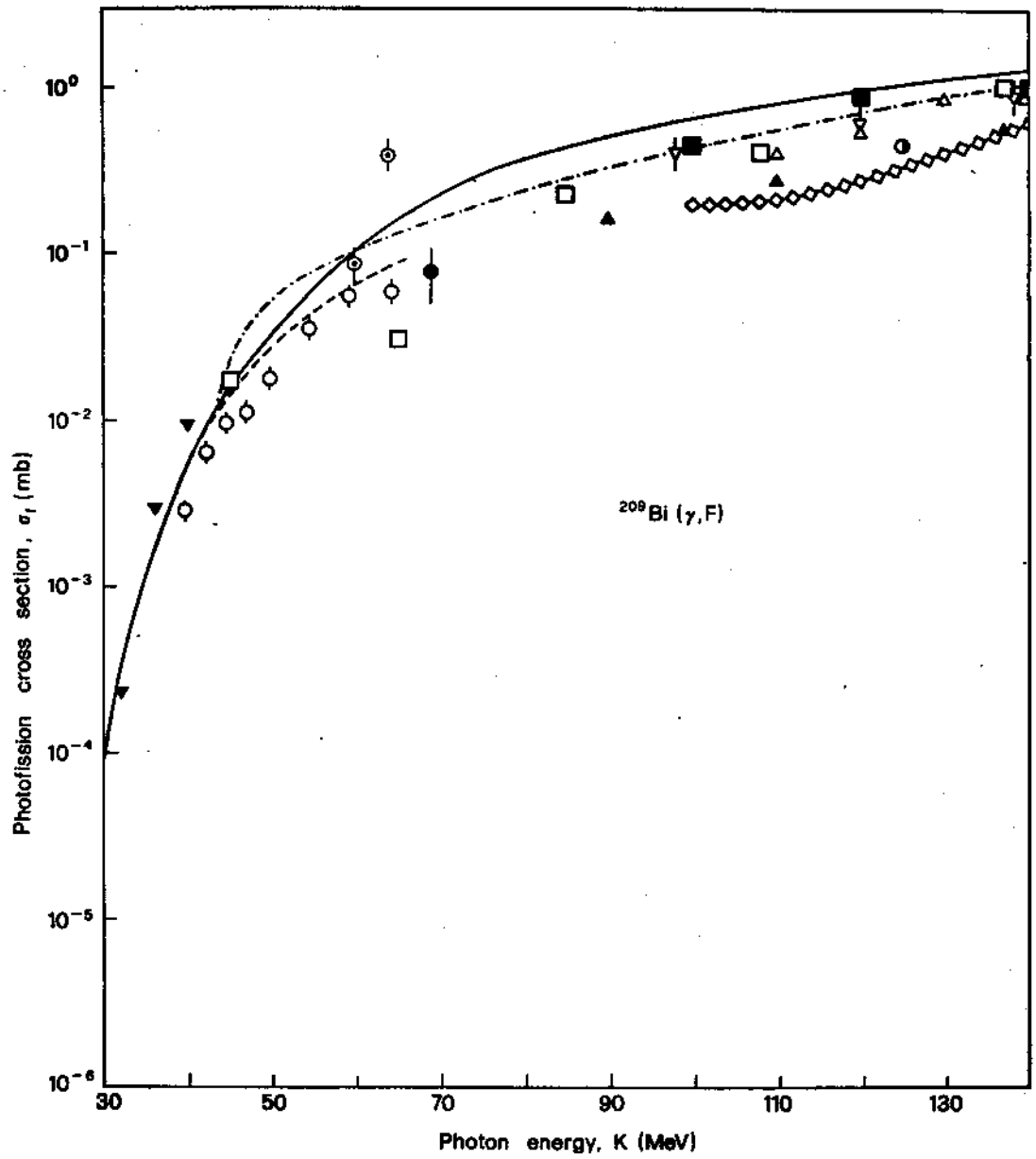
Photofission cross section, σ_f (mb)
10^0
10^{-1}
10^{-2}
10^{-3}
10^{-4}
10^{-5}
10^{-6}
^{209}Bi (γ,F)
30
50
70
90
110
130
Photon energy, K (MeV)

FIG. 9

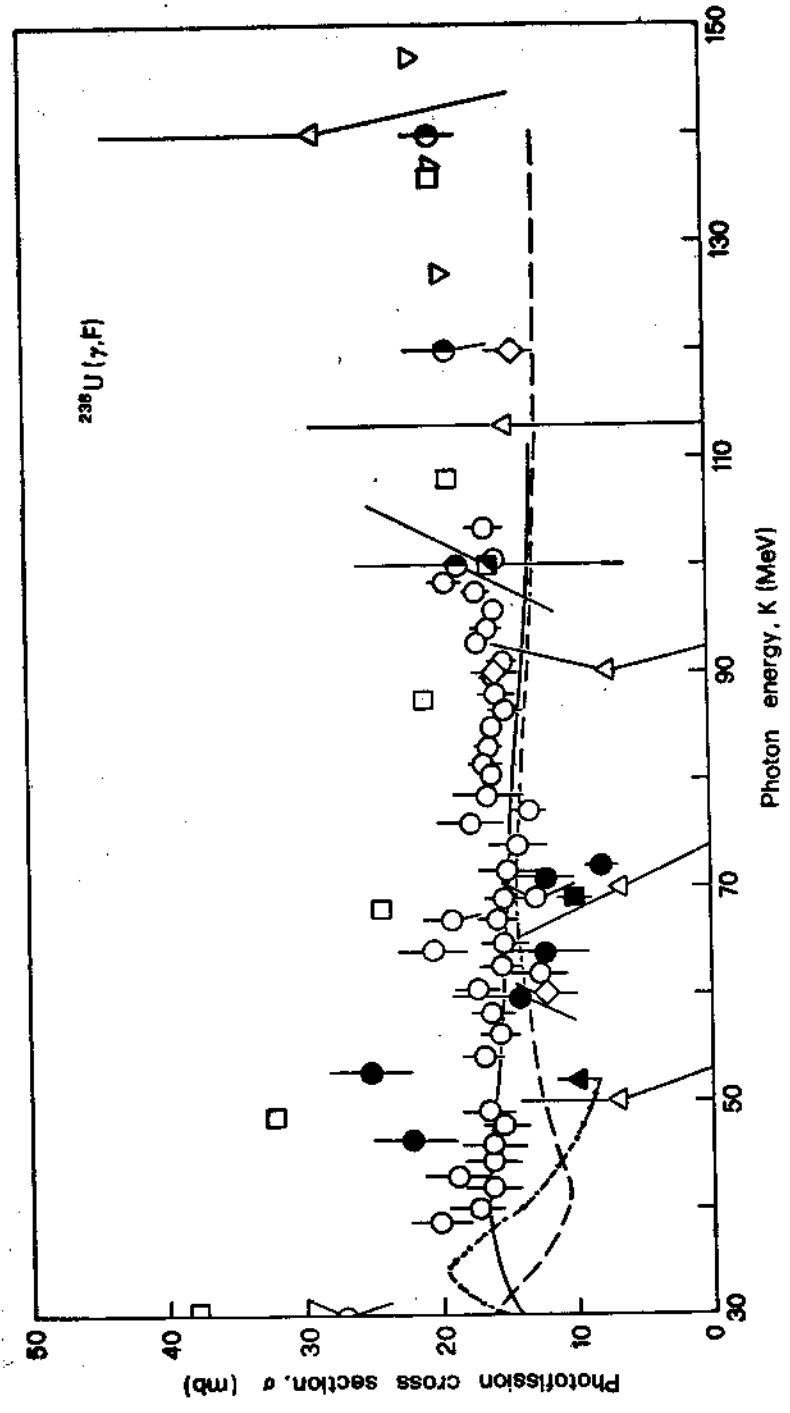
$^{238}U(\gamma,F)$
Photofission cross section, σ (mb)
Photon energy, K (MeV)
0
10
20
30
40
50
30
50
70
90
110
130
150

FIG. 10

Tabel I - Values of the Fermi energy and cut-off energy used in the present analysis.

Target nucleus	Z	A	Nuclear radius R(fm) (+)	Fermi energy E_F (MeV) protons	Fermi energy E_F (MeV) neutrons	Cut-off energy (*) E_C (MeV) protons	Cut-off energy (*) E_C (MeV) neutrons
Bi	83	209	7.126	28.63	37.77	46.78	45.23
U	92	238	7.543	27.37	37.19	50.18	43.34

(+) This is given by $R = (5/3)^{1/2}\langle r^2\rangle^{1/2}$, where values of $\langle r^2\rangle^{1/2}$ are those reported in [34];

(*) The cut-off energy is calculated as the Fermi energy plus the binding energy of the loosest nucleon plus, in the case of protons, the Coulomb energy at surface; binding energy values have been taken from [35].

Table II - Values of the physical quantities used in the present analysis for the different residual nuclei (*).

Target nucleus	Residual nucleus	Binding energy B (MeV)	Ground state fission barrier B_{f_0} (MeV)	Shell correction to the nuclear mass ΔM (MeV)	Neutron separation energy B_n (MeV)	Proton separation energy B_p (MeV)	Alpha separation energy B_α (MeV)	Coulomb barrier at the nuclear surface proton, V_{p_0} (MeV)	Coulomb barrier at the nuclear surface alpha, V_{α_0} (MeV)
^{209}Bi	^{208}Bi	1633	21.66	-11.89	6.89	3.71	-3.05	10.03	20.99
	^{208}Pb	1636	24.36	-13.42	7.37	8.01	-0.52	9.91	20.73
	^{209}Bi	1640	22.37	-12.18	7.46	3.80	-3.14	10.02	20.96
	^{207}Bi	1626	20.99	-10.81	8.10	3.56	-3.28	10.05	21.01
	^{207}Pb	1629	23.68	-13.12	6.74	7.49	-0.39	9.92	20.75
^{238}U	^{237}U	1796	4.88	- 1.43	5.13	7.44	-4.23	10.72	22.54
	^{237}Pa	1794	5.10	- 0.11	5.98	5.40	-3.40	10.60	22.29
	^{238}U	1802	4.92	- 1.04	6.15	7.62	-4.27	10.71	22.51
	^{236}U	1790	4.83	- 1.38	6.54	7.16	-4.57	10.73	22.56
	^{236}Pa	1788	5.09	- 0.45	4.85	6.00	-3.87	10.62	22.31

(*) Values of B, B_n, B_p and B_α are those reported by Wapstra and Audi in their 1983 Atomic Mass Evaluation [35]; Bf_0- and ΔM-values have been obtained from data reported by Myers according to the Droplet Model of the Nucleus [46]; the Coulomb barriers at the nuclear surface (V_{p_0} and V_{α_0}) have been evaluated as explained in the text (see (26) and (27)).

References

1. Nedorezov, V.G.: in Proceedings of the Fourth Course of the International School of Intermediate Energy Nuclear Physics , San Miniato, Italy, 1983, edited by Bergère, R., Costa, S. , Schaerf, C., p. 434. Singapore: World Scientific 1983.

2. Ries, H., Kneissl, U., Mank, G., Stroher, H., Wilke, W., Bergère, R., Bourgeois, P., Carlos, P., Fallou, J.L., Garganne , P., Veyssière, A., Cardman, L.S.: Phys. Lett. 139B,254(1984).

3. Ahrens, J., Arends, J., Bourgeois, P., Carlos, P., Fallou, J. L., Floss, N., Garganne P., Huthmacher, S., Kneissl, U.,Mank, G., Mecking, B., Ries, H., Stenz, R., Veyssière, A.: Phys. Lett. 146B, 303 (1984).

4. Bellini, V., Emma, V., Lo Nigro, S., Milone, C., Pappalardo , G.S., De Sanctis, E., Di Giacomo, P., Guaraldo, C., Lucherini, V., Polli, E., Reolon, A.R.: Nuovo Cimento 85A, 75 (1985).

5. Leprêtre, A., Bergère, R., Bourgeois, P., Carlos, P., Fagot , J., Fallou, J.L., Garganne, P., Veyssière, A., Ries, H., Göbel, R., Kneissl, U., Mank, G., Stroher, H., Wilke, W., Ryckbosch, D., Jury, J.: Nucl. Phys. A472, 533 (1987).

6. Bernabei, R., de Oliveira, V.C., Martins, J.B., Tavares, O.A. P., Pinheiro Filho, J.D., D'Angelo, S., De Pascale, M.P. , Schaerf, C., Girolami, B.: Nuovo Cimento 100A, 131 (1988).

7. Ivanov, D.I., Kezerashvili, G. Ya., Muratov, V.V., Nedorezov, V.G. Sudov, A.S., Zapevalov, V.A.: International Conference , Fiftieth Anniversary of Nuclear Fission, Leningrad (1989).

8. Martins, J.B., Moreira, E.L., Tavares, O.A.P., Vieira, J.L. , Casano, L., D'Angelo, A., Schaerf, C., Terranova, M.L., Babusci, D., Girolami, B.: Phys. Rev. C44, 354 (1991).

9. Tavares, O.A.P., Terranova, M.L., Casano, L., D'Angelo, A. , Moricciani, D., Schaerf, C., Babusci, D., Girolami, B., Martins, J.B., Moreira, E.L., Vieira, J.L.: Phys. Rev. C44, 1683 (1991).

10. Lemke, H.-D., Ziegler, B., Mutterer, M., Theobald,J.P.,Cârjan,

N.: Nucl. Phys. A342, 37 (1980).

11. Bellini, V., Emma, V., Lo Nigro, S., Milone, C., Pappalardo, G.S., De Sanctis, E., Di Giacomo, P., Guaraldo, C., Lucherini, V., Polli, E., Reolon, A.R.: Lett. Nuovo Cimento 36 , 587 (1983).

12. Guaraldo, C., Lucherini, V., De Sanctis, E., Levi Sandri,P., Polli, E., Reolon, A.R., Lo Nigro, S., Aiello, S., Bellini , V., Emma, V., Milone, C., Pappalardo, G.S.: Phys. Rev. C36 , 1027 (1987).

13. Martins, J.B., Moreira, E.L., Tavares, O.A.P., Vieira, J.L., Pinheiro Filho, J.D., Bernabei, R., D'Angelo, S., De Pascale, M.P., Schaerf, C., Girolami, B.: Nuovo Cimento 101 A , 789 (1989).

14. Lucherini, V., Guaraldo, C., De Sanctis, E., Levi Sandri,P., Polli, E., Reolon, A.R., Iljinov, A.S., Lo Nigro, S., Aiello, S., Bellini, V., Emma, V., Milone, C., Pappalardo, G.S., Mebel, M.V.: Phys. Rev. C39, 911 (1989).

15. Levinger, J.S.: Phys. Rev. 84, 43 (1951).

16. Iljinov, A.S., Cherepanov, E.A., Chigrinov, S.E.: Yad. Fiz. 32, 322 (1980) [Sov.J. Nucl. Phys. 32, 166 (1980)].

17. Guaraldo, C., Lucherini, V., De Sanctis, E., Iljinov, A.S. , Mebel, M.V., Lo Nigro, S.: Nuovo Cimento 103A, 607 (1990).

18. Bernardini, G., Reitz, R., Segrè, E.: Phys.Rev. 90,573(1953).

19. Jungerman, J.A., Steiner, H.M.: Phys.Rev. 106, 585 (1957).

20. Minarik, E.V., Novikov, V.A.: Sov. Phys. JETP 5, 253 (1957).

21. Warnock, R.V., Jensen, R.C.: J.inorg.nucl. Chem. 30, 2011 (1968).

22. Vartapetyan, G.A., Demekhina, N.A., Kasilov, V.I., Ranyuk, Yu. N., Sorokin, P.V., Khudaverdyan, A.G.: Yad. Fiz. 14, 65 (1971) [Sov. J. Nucl. Phys. 14, 37 (1972)].

23. Bellini, V., Emma, V., Lo Nigro, S., Milone C., Pappalardo , G.S., Bologna G.: Nuovo Cimento 55A, 182 (1980).

24. Moretto, L.G., Gatti, R.C., Thompson, S.G., Routti, J.T. ,

Heisenberg, J.H., Middleman, L.M., Yearian, M.R., Hofstadter, R.: Phys. Rev. 179, 1176 (1969).

25. Arruda-Neto, J.D.T., Herdade, S.B., Bhandari, B.S., Nascimento, I.C.: Phys. Rev. C14, 1499 (1976).

26. Arruda-Neto, J.D.T., Sugawara, M., Tamae, T., Ogino, H., Miyase, H., Abe, K.: Phys. Rev. C34, 935 (1986).

27. Arruda-Neto, J.D.T., Sugawara, M., Miyase, H., Tobayashi, T., Tamae, T., Abe, K., Yoneama, M.L., Simionatto, S.: Phys.Rev. C41, 354 (1990).

28. Levinger, J.S.: Phys. Lett. 82B, 181 (1979).

29. Terranova, M.L., de Lima, D.A., Pinheiro Filho, J.D.: Europhys. Lett. 9, 523 (1989).

30. Tavares, O.A.P., Terranova, M.L.: J. Phys. G.: Nucl.Part.Phys., in press (1991).

31. Rossi, P., De Sanctis, E., Levi Sandri, P., Bianchi, N.,Guaraldo, C., Lucherini, V., Muccifora, V., Polli, E., Reolon , A.R., Urciuoli, G.M.: Phys. Rev. C40, 2412 (1989).

32. Partovi, F.: Ann. Phys. (N.Y.) 27, 79 (1964).

33. De Pascale, M.P., Giordano, G., Matone, G., Babusci, D., Bernabei, R., Bilaniuk, O.M., Casano, L., D'Angelo, S., Mattioli, M., Picozza P., Prosperi, D., Schaerf, C., Frullani, S., Girolami, B.: Phys. Rev. C32, 1830 (1985).

34. Brown, B.A., Bronk, C.R., Hodgson, P.E.: J. Phys. G.: Nucl. Phys. 10, 1683 (1984).

35. Wapstra, A.H., Audi, G.: Nucl. Phys. A432, 1 (1985).

36. Brueckner, K.A., Serber, R., Watson, K.M.: Phys. Rev. 84, 258 (1951).

37. Forkman, B., Schröder, B.: Phys. Scripta (Sweden)5,105(1972).

38. de Carvalho, H.G., Martins, J.B., Tavares, O.A.P., Nazareth, R.A.M.S., di Napoli, V.: Lett. Nuovo Cimento 2, 1139 (1971).

39. Emets, N.L., Lyubarskii, G. Ya., Ranyuk, Yu. N., Sorokin, P. V.: Preprint KhFTI 72-37, Khar'kov Physico-Technical Institute (1972).

40. Leprêtre, A., Beil, H., Bergère, R., Carlos, P., Fagot, J., Veyssière, A., Halpern I.: Nucl. Phys. A390, 221 (1982).

41. Kikuchi, K., Kawai, M.: Nuclear Matter and Nuclear Reactions 1st Edn. pp. 33-39. Amsterdam: North-Holland 1968.

42. Metropolis, N., Bivins, R., Storm, M., Turkevich, A., Miller, J.M., Friedlander, G.: Phys. Rev. 110, 185 (1958).

43. Weisskopf, V.F.: Phys. Rev. 52, 295 (1937).

44. Vandenbosch, R., Huizenga, J.R.: Nuclear Fission 1st Edn.pp. 227-240. New York and London: Academic Press 1973.

45. Fujimoto, Y., Yamaguchi, Y.: Prog. Theor. Phys.5, 76 (1950).

46. Myers, W.D.: Droplet Model of Atomic Nuclei 1st Edn. pp. 35. New York, Washington and London: Plenum 1977.

47. LeCouteur, K.J.: Proc. Phys. Soc. (London) 63A, 259 (1950).

48. Myers, W.D., Schmidt, K.-H.: Nucl.Phys. A410, 61 (1983).

49. Leprêtre, A., Beil, H., Bergère, R., Carlos, P., Fagot, J., De Miniac, A., Veyssière, A.: Nucl. Phys. A367, 237 (1981).